Article

Influencing the Shape Recovery and Thermomechanical Properties of 3DP PLA Using Smart Textile and Boehmite Alumina and Thermochromic Dye Modifiers

Dimakatso Makwakwa [1,2]**, Mpho Phillip Motloung** [1,2]**, Vincent Ojijo** [1]**, Jayita Bandyopadhyay** [1] **and Suprakas Sinha Ray** [1,2,]*

[1] DST-CSIR National Centre for Nanostructured Materials, Council for Scientific and Industrial Research, Pretoria 0001, South Africa

[2] Department of Chemical Sciences, University of Johannesburg, Doornfontein, Johannesburg 2028, South Africa

* Correspondence: rsuprakas@csir.co.za

Abstract: The technology of 4DP utilizes shape memory materials (SMMs). Among the SMMs, SMP is the material that has potential and is ideal for this technology. However, due to their restrictions, fillers are incorporated to produce a novel shape memory polymer composite (SMPC). The objective of the present work was to investigate how the modification of PLA via the incorporation of boehmite alumina and thermochromic dye, and the use of 3DP on polyester fabric to make smart material textiles (SMT), influenced the shape-memory properties of printed objects. SMPCs with 3 wt% BA particles were prepared by means of the fused deposition modelling (FDM) process, with heat used as an actuation. It was demonstrated that sample thickness and the method of PLA modification affected the shape recovery of 3D-printed objects. All neat PLA samples recovered their angle fully for all thicknesses, while modified PLA incorporated with BA particles and dye recovered its initial angle fully at 1 mm thickness and showed less recovery for 1.5- and 2 mm-thicknesses. The 1 mm-thick sample was then chosen for printing onto the textile material for all samples. When printed onto the fabric, the neat PLA and SMPCs recovered their initial shapes fully, while samples with the dye added into the PLA and SMPC did not recover their initial shape fully due to the presence of the dye, which hindered the movement of the polymer chains. SEM revealed good layer bonding for the SMPCs compared to the neat PLA, which led to improved mechanical properties. The thermal stability of PLA was improved by the BA particles; furthermore, the dye and BA particles nucleated the crystallization of PLA, resulting in an enhanced storage modulus. Overall, a biodegradable 3D-printed object of 1 mm in thickness with improved thermal and mechanical properties was produced, with and without the use of the textile.

Keywords: fused deposition modelling; shape memory polymers; smart material textiles; shape memory materials; shape memory polymer composite; 3D printing; 4D printing; stimulus

1. Introduction

The technology of 3D printing (3DP) (also referred to as additive manufacturing (AM)) is a technique that can develop desired complex structures [1,2]. The technology of 3DP has expanded its application areas to include, biotechnology, custom design and manufacturing, and construction among others since its establishment in the 1980s [3–5]. This technology has advantages such as the ability to decrease tooling costs for better productivity, waste, and easy usage [6]. Regardless of its exceptional pros, 3DP has drawbacks including static parts that cannot be transformed in their shape and difficulty maintaining its rigidity [3]. There are numerous techniques and methods used to produce 3D-printed objects, including stereolithography (SLA), digital light processing (DLP), selective laser melting (SLM), selective laser sintering (SLS), electron beam melting (EBM) and laminated object manufacturing

(LOM) and fused deposition modelling (FDM) [7]. FDM is the most used technology due to its high speed, simplicity, ability to print a wide range of engineering thermoplastics, and is a cost-effective way of producing 3D objects [7,8].

The post-processing of the 3D printed materials can be advantageous for the printing of multiple components, which can then be assembled when needed, for instance, to make an actuating component. Post-3DP, also referred to as 4D printing (4DP), is defined as 3DP with the fourth dimension denoted as time, where the properties of the 3D printed components can change as a function of time [9]. The 4DP technology allows for the use of smart memory materials (SMM) that can change shape and volume when external stimuli, such as heat, chemicals, light and water, are applied to them [10]. However, heat [11], water [12–14], and light [15] are potential stimuli that can cause SMPs to recover their original shape after deformation. Therefore, this study used heat as a stimulus to activate the shape change. Generally, heat-responsive SMPs can be defined by one of the following fundamental mechanisms, (i) dual composite (DCM), (ii) dual-state (DSM), and (iii) partial transition (PTM) mechanisms [16]. Furthermore, this technology has the ability to decrease the processing time and energy needed for the volume of the parts that must be transported and permits the smart material (SM) to be merged with textile materials [17]. This combination of the textile materials and the SM enhances the design properties, especially when producing actuating parts. The 3D printed parts using the smart material act as the activating zone of the component, and the static material acts as the rigid structure of the component that maintains its shape. Areas with the smart material will react and actuate when exposed to stimuli as opposed to the entire component reacting and transforming.

Amongst the SMMs, the shape memory polymers (SMPs) are the most favorable materials due to their high strain recovery, light weight, capability of reacting to various stimuli, ease of printability, and use for a wide range of thermoplastics [10,18]. Recently, biodegradable polymers have also gained interest in shape memory applications. Supported by the growing number of literature reports, polylactide (PLA) has gained immense interest as an SMP [3,19,20]. Leist et al. [3] investigated the shape memory properties of 4D printing using solely PLA when it is joined with the nylon fabric to create the smart textiles material (STM). Their samples were produced with a width of 10 mm, a length of 40 mm, and different thicknesses (800, 1000, and 1200 μm) and with water at temperatures of 65, 75, and 85 °C to be used as an actuator. The authors revealed that irrespective of the thickness, the mean angle of curvature increases with increasing temperature. Higher temperatures and thinner 3D-printed materials bring together the most suitable conditions for fast-reacting smart materials and are more likely to return to their original permanent shape quicker. Mehrpouya et al. [19] reported an investigation on the functionality of thermoresponsive origami structures using PLA as an SMP, and the activation temperatures were 65–75 °C. Their samples were printed with a 100% infilling density, a printing bed temperature of 40 °C, and a printing speed and travel speed of 50 and 100 mm/s, respectively. Their results revealed that an activation temperature of 65 °C promotes a recovery ratio of 85%. When the temperature increases to 75 °C, full shape recovery was observed. Moreover, they noted that the increase in the total thickness of the specimens from 0.9 to 1.5 mm promoted a recovery ratio of 5% lower due to the higher accumulation of imperfections. The total thicknesses can influence the activation time; however, the maximum recovery was reached almost at the same time. Finally, these authors observed that the activation temperature had a significant influence on the shape recovery of origami structures due to the higher heat transfer rate and lower viscosity of the PLA at higher temperatures. Liu et al. [20], reported 4D-printed anisotropic structures with tailored mechanical behaviors and shape memory effects. The authors observed a shape-recovery ratio of more than 91% with the presence of water resistance and a shape-fixity ratio of more than 99.7% after 20 h at room temperature. Overall, the studies showed that using an SMP alone does not lead to the full recovery.

Generally, the incorporation of fillers, including carbon nano tube (CNT) graphene, are used to improve the mechanical and thermal properties of the SMP, leading to the improvement and expansion of the actuation such as electromagnetic, thermal, etc., of the SMP [21,22]. Despite all the benefits from of fillers, their agglomeration can be disadvantageous due to their high aspect ratio and van der Waals interaction [23,24]. To mitigate this phenomenon, chemical and physical methods can be implemented [24]. Lu et al. [25] reported the surface coating of multi-walled carbon nanotube nanopaper on shape-memory polymer for multifunctionalization. The authors created a self-supporting network of the CNT nanopaper by mixing it with solvent, and indeed the SMP nanocomposite was successfully fabricated via a resin transfer molding process. Leng et al. [26] reported an electroactivated shape-memory polymer filled with nanocarbon particles and short carbon fibers. Their results revealed that after grafting CNTs onto the short carbon nano fibers (CNF) for covalent linking, the transfer was improved, meaning the electrical actuation was improved.

Boehmite (BA) particles exhibit interesting properties such as a high surface area, flame retardancy, high thermal stability, and thermal conductivity [27]. Due to this, BA has been included in various polymers to enhance their thermal conductive, flame retardancy, and thermal stability. In a previous study [28], a PLA-based composite containing BA particles at varying concentrations was prepared via melt extrusion. An optimized dispersion was obtained for a 3 wt.% BA content for PLA, which was structurally modified with chain extenders (Joncryl ADR 4368) and dicumyl peroxide (DCP). The better dispersion in the composite containing 3 wt.% BA led to a significant improvement in its mechanical properties. Moreover, the 3D printability of the prepared PLA/J/DCP/BA3 (containing 3 wt% BA) was investigated and it was discernible that the prepared composite could be used in 3D printing for various items. Herein, we further investigated the shape-memory properties of PLA/J/DCP/BA3 and PLA/J/DCP/BA3 composites containing thermochromic dye. The composites were 3D printed with different thicknesses. Then, the composites with the best recovery (based on thicknesses) were further printed onto polyester fabric. The objective of this study was to investigate the effect of BA particles and dye on the 4-dimensional shape memory behavior of PLA printed onto fabric and without the fabric.

2. Materials and Methods

2.1. Materials

The PLA used in this work was of a commercial grade (PLA 4032D), purchased from NatureWorks, LLC (Minnetonka, Plymouth, MN, USA) with a melt flow index (MFI) of 6 g/10 min at 190 °C and a density of 1.23 g cm^{-3}, and BA powder was commercial grade manufactured by SASOL, under the trade name Dispersal 40, containing 80% Al$_2$O$_3$, donated by SASOL Anckelmannspl, Hamburg, Germany. DCP as an initiator was obtained from Sigma-Aldrich (Pomona AH, Kempton Park, South Africa) with a molecular weight of 270.37 g/mol, density of 1056 g/mL, vapor pressure of 15.4 mmHg, and a melting point between 39–41 °C; the chain extender Joncryl ADR 4368 CS was donated by BASF (Chloorkop, Midrand, South Africa). 1.3-dihydro-1.3.3-trimethyl-6-nitrospiro [2H-1-nenzopyran-2.2.(2H) -indole] as a dye was purchased from Sigma-Aldrich (Pomona AH, Kempton Park, South Africa), with a molecular weight of 322.36 g/mol, a melting point between 179–180 °C; remarkably, the thermal stability of the dye was sufficient to process at 190 ° C during melt extrusion, otherwise the use of the organic dye would have been hindered. The polyester fabric used was 0.95 mm thick with a rolled shape to strengthen the mechanical and functional properties of PLA.

2.2. Preparations of the Samples

Filaments: Pulverized PLA powder was dried for 12 h at 80 °C prior to extrusion. Four samples were prepared; neat PLA; 3wt% BA composite, PLA/DCP/J/BA3 (BA3); 0.4wt% dye containing PLA (PLA/dye), and dye containing composite, BA3/dye. All

the samples were melt-mixed in a co-rotating twin-screw extruder from Thermo Scientific, Waltham, MA, USA with L/D of 40. The conditions for the extruder were as follows: feeding rate 5.6 g/min; screw speed 202 rpm; and barrel temperatures from the hopper to the die were 140, 160, 180, 180, 180, 180, 180, 180, 190 °C, respectively. Consequently, the neat PLA and BA composite filaments were produced to a thickness of about 1.5–1.7 mm.

FDM printing: a desktop printer (Wanhao Dupilcator i3 plus) with a 0.4mm nozzle was used to produce the 3D-printed dog bone and DMA specimens. The printing conditions were as follows: nozzle temperature 210 °C, bed temperature 50 °C, print speed of 60 mm/s, 1 perimeter wall, 2 top and bottom layers, and a layer height of 0.2 mm, were printed on a stretchable 0.95 mm polyester fabric. The composite and the dye samples were printed on a stretchable 0.95 mm polyester fabric.

2.3. Techniques Used

The surface morphology of all samples was studied using scanning electron microscopy (SEM) (JSM-7500; JEOL, Japan) at an accelerating voltage of 10.0 kV. The cryo-fractured surfaces of the dynamic mechanical analysis (DMA) specimens were sputter coated with a gold/palladium alloy to avoid charging (and for possible conduction) before being imaged with SEM. Tensile tests were performed to determine the modulus, yield strength, and elongation at the break of each material using an Instron 5966 tester (Instron Engineering Corp., Norwood, MA USA) with a load cell of 10 kN, according to ASTM 638D standards. The test was carried out under tension mode at a single strain rate of 5 mm/min at room temperature. The DMA was conducted using a PerkinElmer DMA analyzer (Model 8000, Branford, CT, USA) analyzer in the dual cantilever-bending mode. The temperature dependence of the storage modulus (E′) was measured at a frequency of 1 Hz, with a strain amplitude of 0.01%, and a heating rate of 2 °C/min in the temperature range of −80 to +115 °C. Differential scanning calorimetry (DSC) measurements were studied using a DSC-Q2000 instrument from TA Instruments, New Castle, DE, USA. Pellets with a mass of approximately 4–5 mg were heated from −20 °C to 190 °C at a rate of 10 °C/min, and then kept constant for 5 min. The samples were cooled to −20 °C at a rate of 10 °C/min and kept constant for 5 min, then heated to 190 °C at a rate of 10 °C/min. Heating and cooling cycles were conducted under nitrogen as the purge gas using a flow rate of 25 mL/min for all samples. The glass transition temperature (T_g), melting temperature T_m, enthalpy of fusion (ΔH_m), crystallization temperature T_c, cold crystallization temperature (T_{cc}) and enthalpy of cold crystallization (ΔH_{cc}) were obtained. The thermogravimetric analyzes were carried out on a TG analyzer (model Q500) from TA Instruments, USA. Samples weighing 10 mg were heated to 900 °C at a rate of 10 °C/min under air with a flow rate of 60 mL/min and a nitrogen flow rate of 40 mL/min. The 3D-printed disc specimens were used for XRD analysis using an X'pert PRO diffractometer from PANalytical (EA Almelo, The Netherlands).

3. Results and Discussion

3.1. Thermal Properties of the Produced Filaments

Generally, the properties of polymers are affected by the formation of crystalline structures and the crystallinity indices upon heating and cooling. The BA particles and dye tend to affect the thermal properties of PLA because of the heat experienced by the material in the melt extruder and during the FDM processes. The effects of the BA particles and the dye on the crystallization and melting temperature (T_m) of the produced filaments and 3D-printed samples were studied for the neat PLA, PLA/dye, BA3, and BA3/dye, denoted as PLA_3dp PLA/DCP/J_3dp, and BA3_3dp, by DSC. The DSC data are summarized in Table 1. The degree of crystallinity (χ_c) during cold crystallization and heating (χ_{cc}) and the total crystallinity (χ_m) were calculated using the following equations [29,30].

$$X_c = \frac{\Delta H_m}{\varnothing_{PLA}\Delta H_c^{\circ}} \times 100; X_{cc} = \frac{\Delta H_m}{\varnothing_{PLA}\,\Delta H_{cc}^{\circ}} \times 100 \tag{1}$$

$$X_m = X_c + X_{cc} \tag{2}$$

where ΔH_m is the melting enthalpy, $\Delta H^{\circ}{}_{cc}$ is the enthalpy of cold crystallization, ØPLA is the weight fraction of PLA, and $\Delta H^{\circ}{}_m$ is the enthalpy of fusion of 100% PLA, assumed as 93.7 J/g [31].

Table 1. DSC of neat PLA, PLA/dye, BA3, and BA3/dye.

Sample Name	T_{cc} (°C)	ΔH_{cc}	X_{cc} (%)	T_m (°C)	ΔH_m	X_m (%)	X_c (%)
Neat PLA_3dp	106.7 ± 0.3	35.6 ± 1.5	36.59	167.3 ± 0.4	38.0 ± 0.8	39.05	2.47
BA3_3dp	106.0 ± 0.7	32.3 ± 1.9	34.36	167.4 ± 0.8	37.0 ± 0.6	39.68	5.32
PLA/Dye_3dp	107.0 ± 2.2	33.6 ± 1.7	35.60	167.5 ± 0.9	36.5 ± 0.3	38.67	3.07
BA3/Dye_3dp	109.0 ± 0.5	32.7 ± 1.1	33.91	167.4 ± 0.5	40.3 ± 0.9	41.79	7.88

Figure 1 shows the micrographs of all the samples, and the summary in Table 1 shows the DSC results from the second heating. In our previous study [28], the inclusion of DCP as an initiator and Joncryl as a chain extender resulted in a better distribution of 3 wt% BA particles, leading to moderate mechanical properties, when compared to that of other composites. Hence, 3 wt% was chosen for further studies. The effects of the processing cycles and the incorporation of 3 wt% BA particles and dye on PLA properties were studied. The pristine PLA filaments have a cold crystallization temperature (T_{cc}) of 110 °C and a T_m of 169 °C. The 3D-printed sample of neat PLA exhibits a decrease in T_{cc} to 106.7 °C compared to that of the filaments (110.2 °C). The T_m of the 3D-printed neat PLA decreased to 167.3 °C, compared to 169 °C for the neat PLA filament.
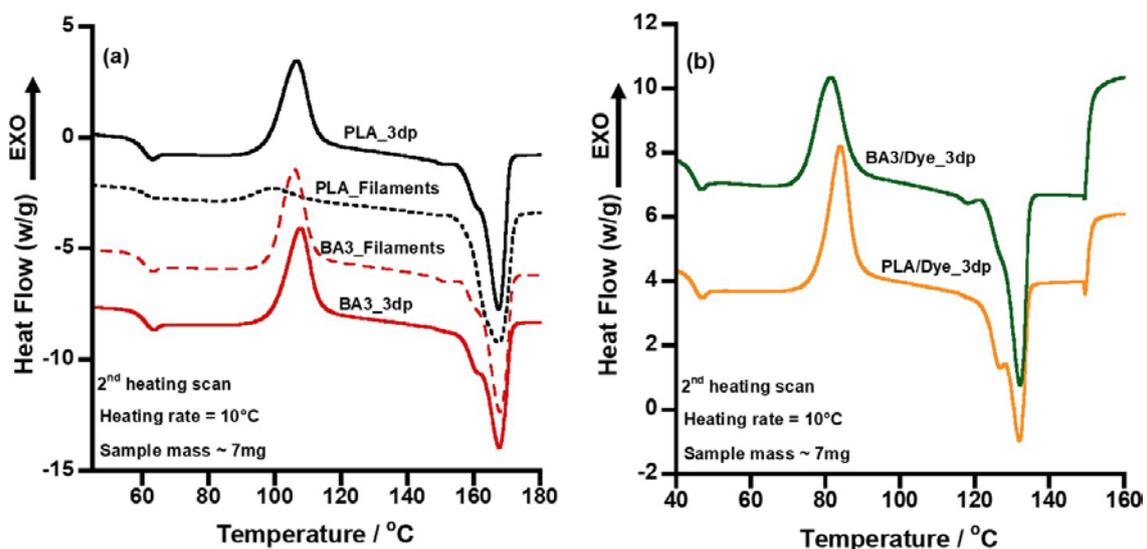

Figure 1. DSC graphs of (**a**) neat PLA filaments, 3d printed neat PLA, BA3 filaments, 3d printed BA3 dye and (**b**) PLA-dye, BA3-Dye.

Upon adding 3 wt% BA particles, the T_{cc} of the filaments decreased from 110.2 to 106 °C. A similar trend was observed for the T_{cc} of the 3D-printed sample (106.0 °C). In the case of the 0.4% dye inclusion, the PLA T_{cc} decreased from 110.2 to 105.9 °C for filaments due to the nucleating effect of the dye. However, there is no significant change in the crystallinity of BA3 and BA3/dye filaments due to the presence of fairly distributed BA particles, which retard PLA crystallization. The processing temperature and processing cycles resulted in a decrease in the T_{cc} for the 3D printed samples compared to the filament samples. No significant changes in the T_{cc} of the 3D-printed samples were observed after adding DCP, Joncryl, and BA particles to the structure of PLA; that is, the T_{cc} of the printed samples compared to that of their neat PLA due to the weak nucleating effect. The BA

particles also acted as good nucleates but with a small crystallinity of 5.32%, as they restrict the mobility of the PLA chain. In summary, the BA particles acted as nucleating agents in contrast to the dyes, with no significant changes in the crystallinity and melting temperature of the PLA.

The 3D-printed XRD patterns of neat PLA, BA3, PLA/dye, and BA3/dye are shown in Figure 2. The XRD patterns of the 3D-printed PLA revealed a halo peak around 15.9°, with a crystallinity of 34.68%. In the case of BA3, the halo peak shifted to a higher angle of 16.9°, suggesting an increase in the crystallinity (37.09%) of the PLA. When the dye was added to the neat PLA, the halo peak moved to a lower angle (15.61°) compared to the neat PLA, suggesting that the dye acted as a nucleating agent, decreasing the crystallinity (33.84%) of the PLA; these results connote the DSC results discussed in the previous section. Interestingly, a synergetic effect of two sharp peaks was observed at 16.6 and 18.6° when the dye was added to the BA3 sample, showing an increase in PLA crystallinity (79.57%), demonstrating that the structure of PLA is holocrystalline [32]. The increase in crystallinity in the PLA structure was due to the nucleating effect of both BA particles and the dye that improved the crystallinity of PLA [33]. The crystallinity of the samples was calculated using the following equation:

$$crystallinity\ index = \left\{ \left(I_{crystalline} - I_{amorphous} \right) \middle| I_{crystalline} \right\} \times 100 \tag{3}$$

where $I_{crystalline}$ is the maximum intensity of the crystalline region of PLA and $I_{amorphous}$ is the intensity of the amorphous region of PLA [34].
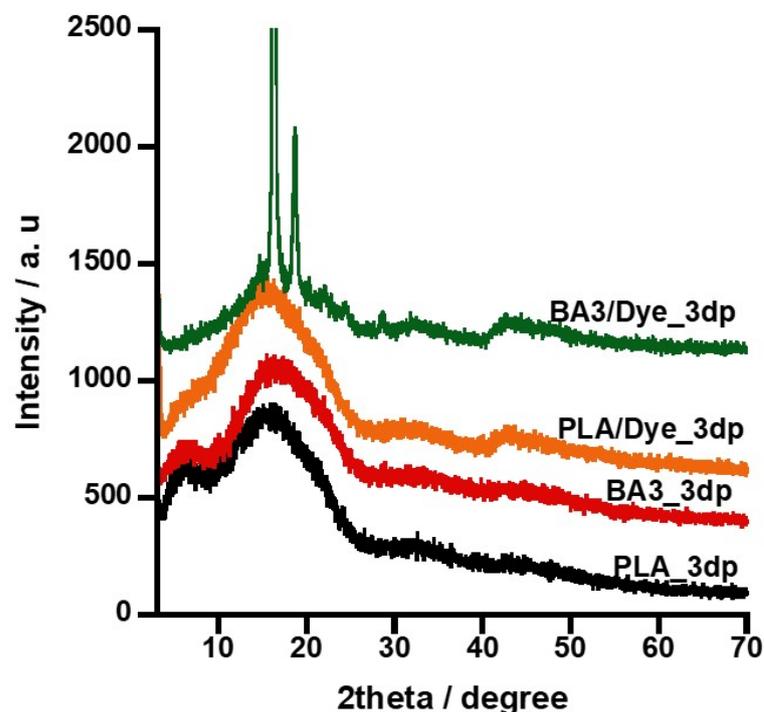

Figure 2. XRD graphs of 3D-printed neat PLA, PLA/dye, BA3, and BA3/Dye.

The thermal degradation characteristics of all the filaments and 3D-printed samples were studied by TGA to evaluate the effect of the dye and BA particles on the PLA. The onset degradation ($T_{0.05}$) was defined as the temperature at which 5% degradation occurred, and the maximum temperature (T_{max}) as that where maximum degradation occurred. The TGA results are plotted in Figure 3 and summarized in Table 2. The figure shows the curves for neat PLA, PLA/dye, BA3, and BA3/dye. The filaments of neat PLA and the neat dye undergo a single-step degradation, with the temperatures being 311.19 and 214.07 °C, respectively, whereas neat BA has two-step degradation temperatures at 59 and 436 °C. The

inclusion of the dye in the PLA matrix improves the thermal stability by 15.1 °C relative to neat PLA. The BA3 sample exhibits the highest thermal stability increase of 27.9 °C. Upon adding the dye to the BA3 sample, the thermal stability of PLA decreased by 14.2 °C. The improvement in the thermal stability is attributed to the BA particles functioning as heat barriers and restricting the PLA chain movement; thereby, the dehydrating process delays the polymer degradation [35]. In the case of FDM-printed samples, the neat PLA and BA3 samples exhibit a single-step degradation at 330.3 and 334.0 °C, respectively. The inclusion of BA particles upshifts the weight loss and DTGA graphs by 4 °C. The observed increase in the thermal stability of PLA upon the addition of BA particles is minimal because of the hindrance of gas transport by BA and low-density pores in BA3, this will be discussed later in Section 3.4. Overall, the inclusion of BA in the PLA matrix improves the thermal stability, whereas the addition of dye does not cause any significant improvement.
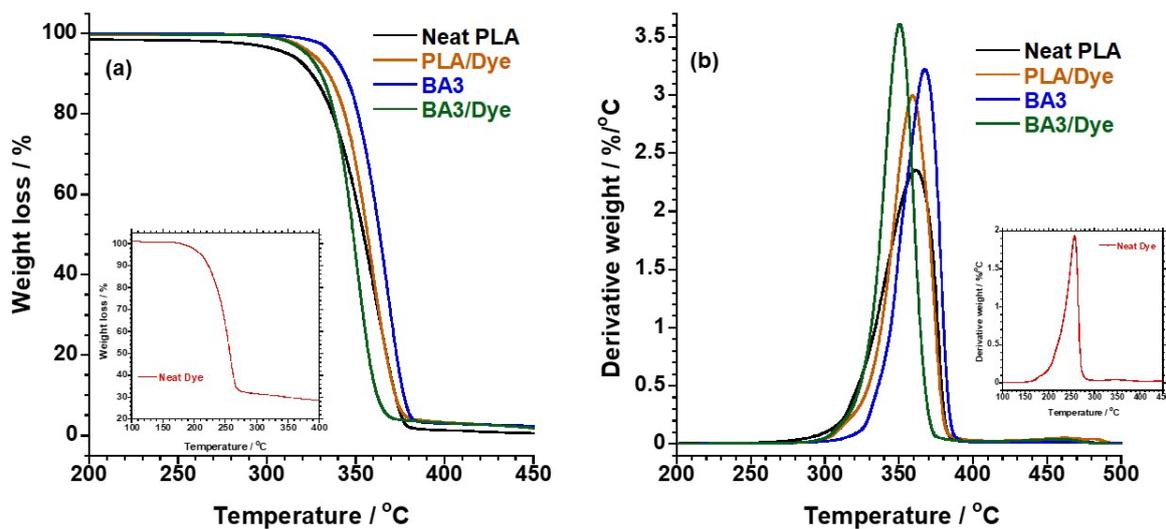

Figure 3. (**a**)TGA and (**b**) DTGA graphs of neat PLA, neat dye, PLA/dye, BA3, and BA3/Dye under nitrogen atmosphere.

Table 2. Onset degradation temperature, $T_{0.05}$, and maximum degradation temperature, T_{max}, of neat PLA, neat Dye, neat BA, PLA/Dye, BA3, and BA3/Dye filaments and 3DP neat PLA and BA3.

Sample Name	$T_{0.05}$ (°C)	T_{max} (°C)
Neat PLA	311.2	361.6
Dye	214.1	260.0
BA	59.0	436.0
PLA/dye	326.3	360.0
BA3	339.1	371.3
BA3/dye	324.9	353.4
PLA_3dp	330.3	360.2
BA3_3dp	334.0	364.4

3.2. Shape Memory Properties of Neat and Modified PLA

Herein, the effects of partial thickness and the PLA-modification method on the shape memory of 3DP parts are discussed. The aim is to optimize the thickness of the 3DP specimen to enable complete initial-shape recovery for both neat and structurally modified PLA in the presence of the dye and 3 wt% BA particles. The 3D-printed specimens for the neat PLA, PLA/DCP/J, PLA/dye, PLA/DCP/J/BA3, and PLA/DCP/J/BA3/dye samples, each with dimensions of 50 mm length, 10 mm width, and 1.0, 1.5, and 2.0 mm thicknesses, were studied for their shape memory properties. The specimens were printed flat, with the infill direction running unidirectionally to the length in the XY'Z direction, where Y' denotes

the infill angle of the 90° raster angle, running parallel to the length of the outline, as shown in Figure 4. Increasing the thickness of the specimen results in a corresponding increase in the printing time and specimen weight during 3D printing. All differently thick samples were heated in a conventional oven at 80 °C for 1 min, subsequently bent to 90° manually, and then were cooled to room temperature to maintain the temporary deformation. For the 2 mm thick specimen, 2 min of conditioning time was required as the cantilevers were not sufficiently pliable after 1 min heating. Afterwards, the specimens were transferred again to the oven and heated above T_g (80 °C) to achieve shape recovery (see Figure 5). The recovery angle was measured using a protractor, and the percentage (%) angular shape recovery was calculated using Equation 4. The test was conducted in triplicate for reproducibility.

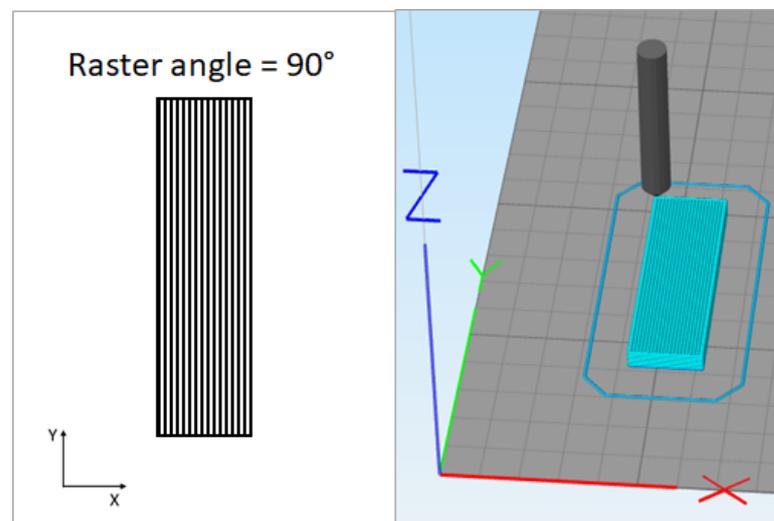$$R\%_{angle} = \frac{recovery\ angle}{90} \times 100 \tag{4}$$

Figure 4. Schematic showing the build orientation of the 3D-printed cantilevers.

Figure 5. Shape memory behavior of the 3D-printed PLA specimens: (**a**) initial PLA specimen at 180°; (**b**) programmed specimen (the specimen was heated in a conventional oven at 80 °C for 1 min, then programmed at 90°, and finally cooled to room temperature); (**c**) specimen is reverted to the oven at 80 °C for shape recovery.

Complete shape recovery was observed for PLA specimens for all the thicknesses tested. Mehrpouya et al. [19] reported that PLA samples that are 0.9 to 1.5 mm thick do not recover fully at 65 °C; however, full recovery was observed at 75 °C. In the present study, the actuation temperature was set at 80 °C, which explains the full recovery displayed by the thicker specimens and the differences from those reported by Mehrpouya et al. [19]. When the layer thickness was 2.0 mm, the mass of the PLA sample used was high (8.5 g), with the highest number of layers taking more time to print. In addition, the PLA sample had the highest temperature incline, and the heat transfer rate from the outer layers to the inner layers was the maximum. In the recovery process, under the same experimental conditions, the inner layers of the PLA did not heat faster; hence, the delay in reaching the rubbery state, where the stress deposited in the stretched polymer chains was released, and

a higher shape-recovery ratio was achieved. On the contrary, when the layer thickness was 1.0 mm, this decreased to 6.3 g, with a lower number of layers and less print time, resulting in a lower temperature rise. The inner layers of the PLA sample were heated faster, and less time was required to achieve the rubbery state; thus, the shape recovery rate was high.

On the other hand, for the modified PLA samples, i.e., PLA/dye, PLA/DCP/J, BA3, and BA3/dye, full shape recovery was observed only for the 1.0 mm thick samples. All the modified PLA samples could only partially recover between 177 and 178° when their thicknesses were 1.5 and 2 mm; the trend is shown in Figure 6. The 2 mm thick sample required an additional exposure time of 1 min in the oven for the programming step due to its high mass during printing and the restriction in the movement of the polymer chains due to BA. In the programming step, the sample was heated beyond its T_g (80 °C herein) to initiate the movement of the polymer chain. Overall, during programming, high temperatures are preferred for thin samples to facilitate a quick response with little printing material requirement, thereby increasing the probability of the sample returning to its initial shape (180°). Figure 7 shows the temperature tower for PLA for 3D printing, suggesting that the PLA used in this work can be printed at up to 220 °C.
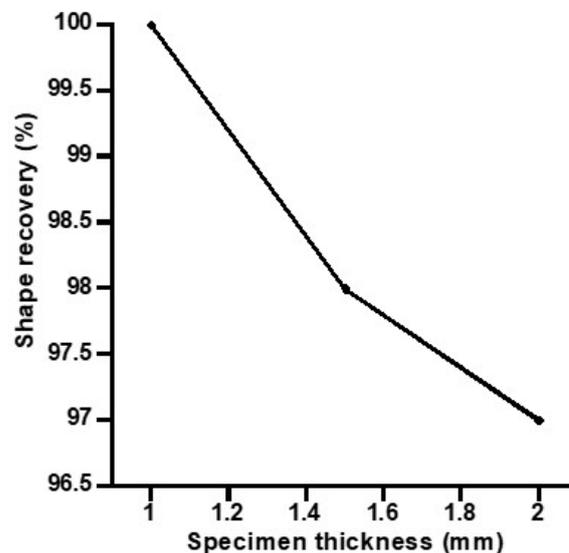

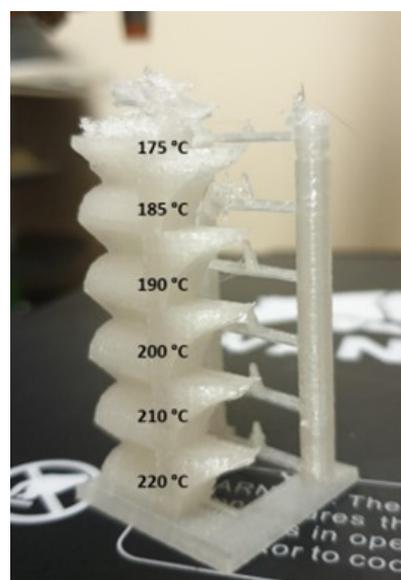**Figure 6.** Dependence of shape recovery on specimen thickness.

Figure 7. Temperature tower for neat PLA.

3.3. The Utility of Smart Textile and PLA Modification in Controlling the Rate and Extent of Shape Recovery of 3DP Objects

The previous section demonstrated that the 3DP neat PLA and BA3 possess a 100% shape memory property for 1 mm-thick objects and that the addition of the dye to neat PLA and BA3 decreases this recovery. By modifying the PLA (for instance, in BA3), both the extent of shape recovery and the mechanical properties can be controlled. A previous study by the same authors inferred that 3 wt% BA increases the tensile modulus of PLA by 8.8% [28], and that the shape recovery of modified PLA is partial. To further control the rate and extent of shape recovery, 3DP was performed on a prestressed rolled-up textile material (STM) to fabricate a smart textile material (STM). STMs are attractive because they combine mechanical and functional properties, which is typical of composites, along with shape memory properties. A 0.95 mm-thick rolled-up fabric was used in this study, as shown in Figure 8. Figure 9a shows the STM mesh design for the neat PLA, PLA/dye, and BA3/dye with their original shapes; the STMs were heated in a conventional oven at 80 °C for 1 min. Figure 9b shows a programmed cylindrical shape, which forms within the preferred prestressed shape of the textile material. Figure 9c reveals the complete recovery of the neat PLA sample for the 3D-mesh-printed objects. Moreover, the BA3 sample exhibits a similar behavior but with better mechanical properties than neat PLA. High temperatures were used to print PLA/dye and BA3/dye as the materials swelled in the nozzle at low temperatures. Further, the PLA/dye and BA3/dye samples do not completely recover their initial angle. (Note: the fabric used herein is stretchable, and when printed upon, it flexes, affecting the generated stresses). The neat PLA and BA3 begin unfolding first from the programmed cylindrical shape, followed by the PLA/dye (after 1 min), and finally by the BA3/dye (after 2 min). The neat PLA, BA3, and PLA/dye have the same unfolding rate despite the delay of the unfolding process caused by the PLA/dye. The BA3/dye has the slowest unfolding rate.

Figure 8. Polyester fabric.

The unfolding rate of the BA3/dye sample is small because of the presence of the three-dimensional arrangement of the azo group in the dye with two configurations, namely, trans (more stable) and cis configurations enable the application of BA3/dye-based materials toward optical storage [29]. Overall, the dye delays the unfolding rate of the samples, and the final product may be used in applications that do not require flat shapes.

3.4. Morphology and Mechanical Properties of the 3D-Printed Components

Figure 10 shows the macrostructure of the 3D-printed samples for neat PLA, PLA/dye, BA3, and BA3/dye. The images were observed from the cross-sectional area of the DMA specimen. All the samples exhibit quasitriangular pores, produced by the deposition of layers during the FDM 3D printing [29]. The structural modification of PLA using DCP and Joncryl and the introduction of BA particles enhances its thermal stability and mechanical properties. Consequently, BA3 and BA3/dye have smaller pores than neat PLA

and PLA/dye samples. The size reduction of the pores is attributed to the good bonding strength between the filament layers [36]. On the other hand, PLA/dye exhibits an interface debonding between adjacent layers with damage evolution, leading to larger pores than those in neat PLA, owing to the poor adhesion and/or inconsistent filament diameter resulting from the extruder. Further, the morphology of BA3 reveals a good layer adhesion due to the good dispersion of the BA particles in the PLA matrix, as observed in our previous work [28]. The addition of the dye to BA3 reduces the pore size. Furthermore, the layer height of the 3D printer was set to 0.2 mm, as discussed previously; however, the layer heights of the 3D-printed components for all samples decreased because of compression buildup during the FDM printing. In summary, the results show that BA3 has good bonding strength between the layer interfaces, leading to enhanced mechanical properties.
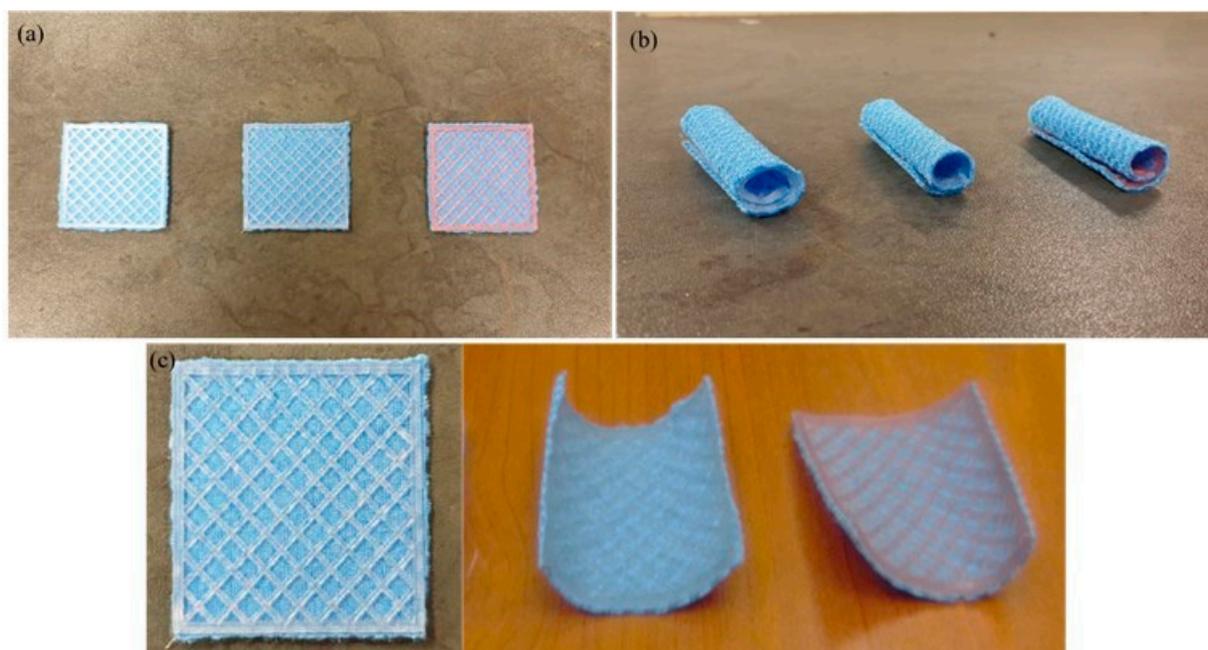

Figure 9. Mesh 3D-printed samples on a polyester fabric. (**a**) 3D printed mesh design on smart material before heating; (**b**) all samples heated at 80 °C for 1 min and then programmed to a cylindrical shape, and (**c**) SMT after the recovery step.

Table 3 summarizes the elastic modulus (E′), elongation at break (εb), and tensile strength (σ) of the 3D-printed components for the neat PLA, PLA/dye, and BA3 composites. The tensile results for the BA3/dye sample have not been included because the material swelled in the nozzle, rendering the dog-bone specimen nonprintable. In the print core, the semi-molten filament is pushed via the nozzle at the defined printing temperature [36]. The polymer melt then undergoes a pressure drop due to the constrained convergence from the filament diameter (df) to the nozzle diameter (dn), resulting in an elongational flow, which can orient both the macromolecular chains and BA particles. Additionally, filament stretching slightly occurs in the semi-molten state, owing to the speed gradient between the filament speed and printing speed. The table shows that the brittle pristine PLA exhibits the lowest E′, εb, and σ. The inclusion of dye did not show any significant change to the mechanical properties of 3DP PLA. However, with the incorporation of BA particles, an increase in E′ and σ was noticed, which implied the reinforcing effect of BA. This phenomenal increase is attributed to the stiffness of the filler, which contributed to resisting the deformation and facilitating an effective stress transfer between the PLA matrix and filler, with good layer adhesion. Consequently, the tensile properties of the PLA increased [37]. Overall, the inclusion of BA particles increased the tensile properties of neat PLA.
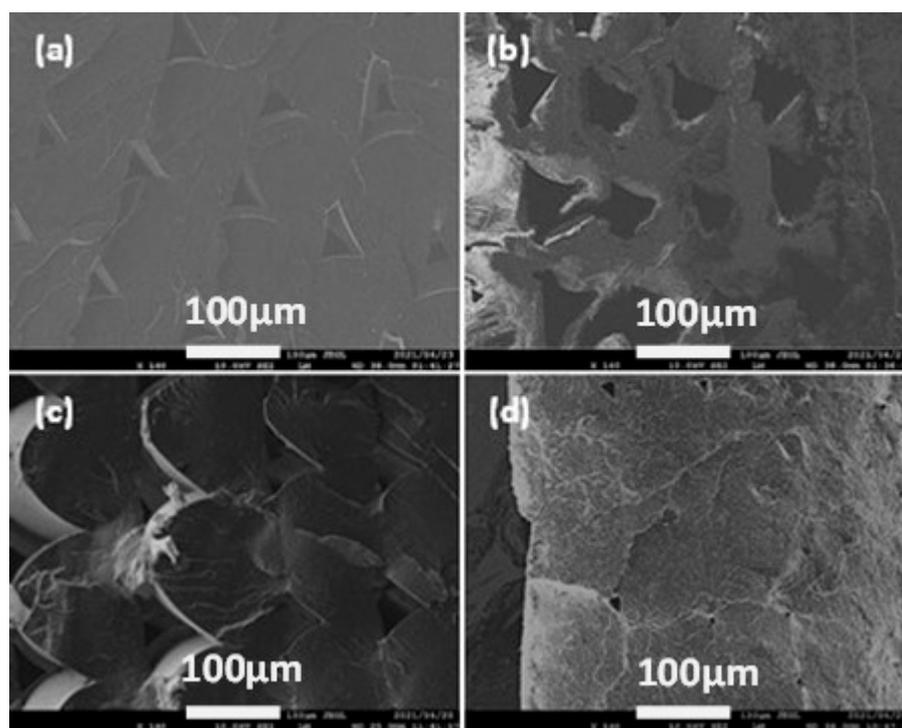
Figure 10. Cryofracture SEM images of the 3D printed components for (**a**) neat PLA; (**b**) PLA/dye; (**c**) BA3, and (**d**) BA3/dye.

Table 3. Tensile properties of the 3D-printed properties for neat PLA, neat Dye, PLA/Dye, and BA3.

Sample Name	Modulus (MPa)	Elongation at Break %	Ultimate Tensile Strength (MPa)
Neat PLA	1470.2 ± 262.79	5.70 ± 0.21	65.25 ± 20.43
PLA/dye	1499.0 ± 233.01	6.01 ± 0.21	69.30 ± 0.91
BA3	1652.3 ± 4031	7.00 ± 0.07	73.05 ± 1.20

The effect of the 3D-printed specimens on the thermomechanical properties of PLA was studied via DMA. Figure 11a displays the storage modulus (E') of the neat PLA, PLA/dye, BA3, and BA3/dye samples as a function of temperature. The E' of all the samples is explained in three diverse regions: (i) the glassy region, below the T_g of the PLA, where the chains are constrained, (ii) the transition region, at the T_g of the PLA (60 °C), where the movement of the polymer chains begins, and (iii) above the T_g of the polymer, between 100 and 110 °C, with this region related to the T_{cc} of the sample from DSC. The first region shows that rigid PLA has the lowest E'. The E' increases upon dye addition, owing to the reinforcing effect and high crystallinity, as inferred from DSC, regardless of the destroyed morphology. On the other hand, the inclusion of BA particles increases the E' PLA matrix. PLA/dye has a much higher E' than neat PLA; this phenomenal increase can be attributed to the high crystallinity of the PLA/dye. These results are consistent with the DSC results shown in Table 1. However, the addition of the dye to BA3 decreases the E' of PLA, possibly because of the disrupted dispersion of the BA particles in the BA3. In the second region, the T_g of the samples is examined; the corresponding tan delta curves are shown in Figure 11b for clearer visualization. The figure reveals that the structural modification of PLA and the inclusion of the dye and BA particles in the PLA matrix slightly upshifts the curve to higher temperatures.
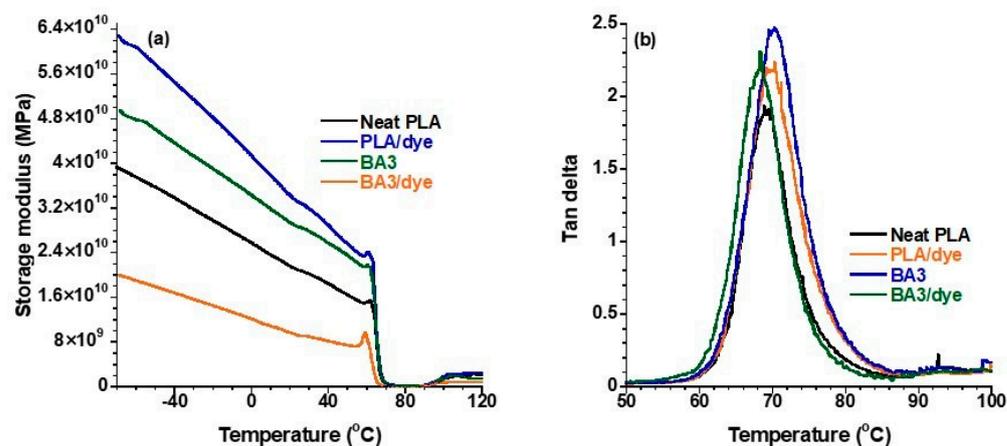
Figure 11. DMA plots for (**a**) storage moduli; (**b**) tan delta curves of neat PLA, PLA/dye, BA3, and BA3/dye.

Table 4 compares the recent studies on the shape memory composite printed via FDM. To the best of our knowledge, there are no studies that report the same system used in this study. Although, other authors have used blends that lead to the higher pricing of the final material produced. Liu et al. [20] reported a higher shape recovery of more than 99.7% for a composite, higher than the one observed in the present study. However, in their case, the shape recovery was carried out with the presence of water assistance for 20 h at room temperature.

Table 4. Shape memory composite printed via FDM by various researchers.

Year	Polymers	Conclusions	Reference
2020	PLA	The authors revealed that low temperatures (65 °C) did not result in full shape recovery but did at higher temperatures (75 °C).	[38]
2019	PCL	The addition of 20 wt.% PCL to the created system, the linear polymer reveals the self-healing capacity to 4D-printed structures, and the improvement of mechanical properties by more than 90%.	[39]
2020	PLA	PLA revealed a shape recovery ratio of more than 91%, with the existence of water resistance and a shape fixity ratio of more than 99.7% after 20 h at room temperature.	[20]
2020	PLA	The authors revealed that the optimal recovery ratio can be attained by using higher activations and nozzle temperatures and lower printing speeds.	[40]
2020	PLA and TPU	When PLA and TPU load is at 80% and 20% weight, the filament revealed the consistent and greatest shape memory characteristics. Maintains good shape fixity and shape recovery ratios, as well as resisting repeated deformation and recovery cycles. PLA has the ability to accelerate and maintain velocity during recovery.	[41]

4. Conclusions

The present study investigates the mechanical, thermal, and morphological properties of the filaments used in FDM printing and the shape-memory properties of the printed samples with and without polyester fabric. We also investigated the potential of PLA modification and the use of prestressed textiles to control the extent and rate of shape recovery for the 3D-printed objects. The objective of this study was to investigate the effect of 3 wt% BA particles and dye on the fourth-dimensional shape memory behavior of PLA printed onto a fabric and without the fabric. The neat PLA samples, with different thicknesses, completely recovered their initial shape. The presence of 3 wt% BA particles and dye resulted in an object with better mechanical and thermal properties than the neat PLA sample, with full recovery at low thicknesses and an exhibited partial recovery at higher thicknesses. For the textile-printed samples, complete recovery was shown by neat PLA and BA3, while partial recovery was shown by PLA samples containing dye and

BA particles samples. The dye and BA particles acted as good nucleating and reinforcing agents for improving the thermal stability of PLA. In general, biodegradable materials with improved properties were produced and printed using FDM.

Institutional Review Board Statement: Not applicable.

Informed Consent Statement: Not applicable.

Data Availability Statement: Not applicable.

Conflicts of Interest: The authors declare no conflict of interest.

References

1. Leng, J.; Lan, X.; Liu, Y.; Du, S. Shape-memory polymers and their composites: Stimulus methods and applications. *Prog. Mater. Sci.* **2011**, *56*, 1077–1135. [CrossRef]
2. Liu, Y.; Lv, H.; Lan, X.; Leng, J.; Du, S. Review of electro-active shape-memory polymer composite. *Compos. Sci. Technol.* **2009**, *69*, 2064–2068. [CrossRef]
3. Leist, S.K.; Gao, D.; Chiou, R.; Zhou, J. Investigating the shape memory properties of 4D printed polylactic acid (PLA) and the concept of 4D printing onto nylon fabrics for the creation of smart textiles. *Virtual Phys. Prototyp.* **2017**, *12*, 290–300. [CrossRef]
4. Berman, B. 3-D printing: The new industrial revolution. *Bus. Horiz.* **2012**, *55*, 155–162. [CrossRef]
5. Huang, S.H.; Liu, P.; Mokasdar, A.; Hou, L. Additive manufacturing and its societal impact: A literature review. *Int. J. Adv. Manuf. Technol.* **2013**, *67*, 1191–1203. [CrossRef]
6. Ramesh, S.; Reddy, S.K.; Usha, C.; Naulakha, N.K.; Adithyakumar, C.R.; Reddy, M.L.K. Advancements in the Research of 4D Printing-A Review. *IOP Conf. Ser. Mater. Sci. Eng.* **2018**, *376*, 012123. [CrossRef]
7. García-Huete, N.; Axpe, E.; Cuevas, J.M.; Mérida, D.; Laza, J.M.; García, J.Á.; Vilas, J.L.; Plazaola, F.; León, L.M. In situ measurements of free volume during recovery process of a shape memory polymer. *Polymer* **2017**, *109*, 66–70. [CrossRef]
8. Liu, Y.; Du, H.; Liu, L.; Leng, J. Shape memory polymers and their composites in aerospace applications: A review. *Smart Mater. Struct.* **2014**, *23*, 023001. [CrossRef]
9. Momeni, F.; Hassani, N.S.M.M.; Liu, X.; Ni, J. A review of 4D printing. *Mater. Des.* **2017**, *122*, 42–79. [CrossRef]
10. Biswas, M.C.; Chakraborty, S.; Bhattacharjee, A.; Mohammed, Z. 4D Printing of Shape Memory Materials for Textiles: Mechanism, Mathematical Modeling, and Challenges. *Adv. Funct. Mater.* **2021**, *31*, 2100257. [CrossRef]
11. González-Jiménez, A.; Bernal-Ortega, P.; Salamanca, F.M.; Valentin, J.L. Shape-Memory Composites Based on Ionic Elastomers. *Polymers* **2022**, *14*, 1230. [CrossRef] [PubMed]
12. Panda, P.K.; Yang, J.-M.; Chang, Y.-H. Water-induced shape memory behavior of poly (vinyl alcohol) and p-coumaric acid-modified water-soluble chitosan blended membrane. *Carbohydr. Polym.* **2021**, *257*, 117633. [CrossRef] [PubMed]
13. Yang, J.M.; Panda, P.K.; Jie, C.J.; Dash, P.; Chang, Y.H. Poly (vinyl alcohol)/chitosan/sodium alginate composite blended membrane: Preparation, characterization, and water-induced shape memory phenomenon. *Polym. Eng. Sci.* **2022**, *62*, 1526–1537. [CrossRef]
14. Panda, P.K.; Dash, P.; Biswal, A.K.; Chang, Y.-H.; Misra, P.K.; Yang, J.-M. Synthesis and Characterization of Modified Poly(vinyl alcohol) Membrane and Study of Its Enhanced Water-Induced Shape-Memory Behavior. *J. Polym. Environ.* **2022**, *30*, 3409–3419. [CrossRef]
15. Sun, Y.-C.; Wan, Y.; Nam, R.; Chu, M.; Naguib, H.E. 4D-printed hybrids with localized shape memory behaviour: Implementation in a functionally graded structure. *Sci. Rep.* **2019**, *9*, 18754. [CrossRef]
16. Ahmed, A.; Arya, S.; Gupta, V.; Furukawa, H.; Khosla, A. 4D printing: Fundamentals, materials, applications and challenges. *Polymer* **2021**, *228*, 123926. [CrossRef]
17. Mitchell, A.; Lafont, U.; Hołyńska, M.; Semprimoschnig, C. Additive manufacturing—A review of 4D printing and future applications. *Addit. Manuf.* **2018**, *24*, 606–626. [CrossRef]
18. Liu, C.; Qin, H.; Mather, P.T. Review of progress in shape-memory polymers. *J. Mater. Chem.* **2007**, *17*, 1543–1558. [CrossRef]
19. Mehrpouya, M.; Azizi, A.; Janbaz, S.; Gisario, A. Investigation on the functionality of thermoresponsive origami structures. *Adv. Eng. Mater.* **2020**, *22*, 2000296. [CrossRef]
20. Liu, T.; Liu, L.; Zeng, C.; Liu, Y.; Leng, J. 4D printed anisotropic structures with tailored mechanical behaviors and shape memory effects. *Compos. Sci. Technol.* **2020**, *186*, 107935. [CrossRef]
21. Zhang, Q.; Yan, D.; Zhang, K.; Hu, G. Pattern transformation of heat-shrinkable polymer by three-dimensional (3D) printing technique. *Sci. Rep.* **2015**, *5*, srep08936. [CrossRef] [PubMed]

22. Liu, T.; Zhou, T.; Yao, Y.; Zhang, F.; Liu, L.; Liu, Y.; Leng, J. Stimulus methods of multi-functional shape memory polymer nanocomposites: A review. *Compos. Part A Appl. Sci. Manuf.* **2017**, *100*, 20–30. [CrossRef]

23. Girifalco, L.A.; Hodak, M.; Lee, R.S. Carbon nanotubes, buckyballs, ropes, and a universal graphitic potential. *Phys. Rev. B* **2000**, *62*, 13104. [CrossRef]

24. Peterson, G.I.; Larsen, M.B.; Ganter, M.A.; Storti, D.W.; Boydston, A.J. 3D-printed mechanochromic materials. *ACS Appl. Mater. Interfaces* **2015**, *7*, 577–583. [CrossRef]

25. Lu, H.; Liu, Y.; Gou, J.J.; Leng, J.; Du, S. Surface coating of multi-walled carbon nanotube nanopaper on shape-memory polymer for multifunctionalization. *Compos. Sci. Technol.* **2011**, *71*, 1427–1434. [CrossRef]

26. Leng, J.; Zhang, D.; Liu, Y.; Yu, K.; Lan, X. Study on the activation of styrene-based shape memory polymer by medium-infrared laser light. *Appl. Phys. Lett.* **2010**, *96*, 111905. [CrossRef]

27. Malwela, T.; Khumalo, V.M.; Salehiyan, R.; Ray, S.S. Characterization of polypropylene/polystyrene boehmite alumina nanocomposites: Impact of filler surface modification on the mechanical, thermal, and rheological properties. *J. Appl. Polym. Sci.* **2018**, *135*, 46376. [CrossRef]

28. Makwakwa, D.; Ojijo, V.; Bandyopadhyay, J.; Ray, S.S. Flow Characteristics, Mechanical, Thermal, and Thermomechanical Properties, and 3D Printability of Biodegradable Polylactide Containing Boehmite at Different Loadings. *Polymers* **2021**, *13*, 2019. [CrossRef]

29. Fleischmann, C.; Lievenbrück, M.; Ritter, H. Polymers and Dyes: Developments and Applications. *Polymers* **2015**, *7*, 717–746. [CrossRef]

30. Das, K.; Ray, S.S.; Chapple, S.; Wesley-Smith, J. Mechanical, Thermal, and Fire Properties of Biodegradable Polylactide/Boehmite Alumina Composites. *Ind. Eng. Chem. Res.* **2013**, *52*, 6083–6091. [CrossRef]

31. Cao, Y.; Sun, T.; Kou, J.; Xu, C.; Gao, E. Effect of Na2CO3 and CaCO3 on coreduction roasting of blast furnace dust and high-phosphorus oolitic hematite. *J. Wuhan Univ. Technol.-Mater. Sci. Ed.* **2017**, *32*, 517–524. [CrossRef]

32. Hamad, K.; Kaseem, M.; Yang, H.; Deri, F.; Ko, Y. Properties and medical applications of polylactic acid: A review. *Express Polym. Lett.* **2015**, *9*, 435–455. [CrossRef]

33. Hosen, M.S.; Rahaman, M.H.; Gafur, M.; Habib, R.; Qadir, M. Preparation and characterization of poly (L-lactic acid)/chitosan/microcrystalline cellulose blends. *Chem. Sci. Int. J.* **2017**, *21*, 1–10. [CrossRef]

34. Orasugh, J.T.; Saha, N.R.; Rana, D.; Sarkar, G.; Mollick, M.M.R.; Chattoapadhyay, A.; Mitra, B.C.; Mondal, D.; Ghosh, S.K.; Chattopadhyay, D. Jute cellulose nano-fibrils/hydroxypropylmethylcellulose nanocomposite: A novel material with potential for application in packaging and transdermal drug delivery system. *Ind. Crop. Prod.* **2018**, *112*, 633–643. [CrossRef]

35. Zhang, J.; Ji, Q.; Zhang, P.; Xia, Y.; Kong, Q. Thermal stability and flame-retardancy mechanism of poly (ethylene terephthalate)/boehmite nanocomposites. *Polym. Degrad. Stab.* **2010**, *95*, 1211–1218. [CrossRef]

36. Fekete, I.; Ronkay, F.; Lendvai, L. Highly toughened blends of poly(lactic acid) (PLA) and natural rubber (NR) for FDM-based 3D printing applications: The effect of composition and infill pattern. *Polym. Test.* **2021**, *99*, 107205. [CrossRef]

37. McIlroy, C.; Olmsted, P.D. Deformation of an amorphous polymer during the fused-filament-fabrication method for additive manufacturing. *J. Rheol.* **2017**, *61*, 379–397. [CrossRef]

38. Harishanand, K.; Nagabhushana, H.; Nagabhushana, B.; Panda, P.; Gupta, R.; Muruli, M.; Raghavendra, N.; Mahesh, K.V. Comparitive study on mechanical properties of ZnO, ZrO2 and CeO2 nanometal oxides reinforced epoxy composites. *Adv. Polym. Sci. Technol. Int. J* **2013**, *3*, 7–13.

39. Zhang, B.; Zhang, W.; Zhang, Z.; Zhang, Y.-F.; Hingorani, H.; Liu, Z.; Liu, J.; Ge, Q. Self-healing four-dimensional printing with an ultraviolet curable double-network shape memory polymer system. *ACS Appl. Mater. Interfaces* **2019**, *11*, 10328–10336. [CrossRef]

40. Mehrpouya, M.; Gisario, A.; Azizi, A.; Barletta, M. Investigation on shape recovery of 3D printed honeycomb sandwich structure. *Polym. Adv. Technol.* **2020**, *31*, 3361–3365. [CrossRef]

41. Carlson, M.; Li, Y. Development and kinetic evaluation of a low-cost temperature-sensitive shape memory polymer for 4-dimensional printing. *Int. J. Adv. Manuf. Technol.* **2020**, *106*, 4263–4279. [CrossRef]